CrossMark

ORIGINAL ARTICLE

An annually-resolved stem growth tool based on 3D laser scans and 2D tree-ring data

Bettina Wagner[1] · Christian Ginzler[1] · Anton Bürgi[1] · Silvia Santini[2] ·
Holger Gärtner[1]

Abstract

Key message **The combination of terrestrial laser scans and tree-ring data allows for a highly precise reconstruction of annual stem growth, and thus complex tree-growth analyses independent of species and site characteristics.**

Abstract Reliable carbon pools data are needed to quantify the carbon stored in ecosystems and for effective forest management. Terrestrial laser scanning allows researchers to quickly acquire data about forest structure and to derive tree parameters and volume data automatically. However, accurate models of the development of tree volume over time are still lacking. In contrast to terrestrial laser scanning, tree-ring data show the annual growth development of trees, but do not contain information about tree volume. The fusion of terrestrial laser scanning and tree-ring data may, therefore, lead to reliable stem development data, and thus annually resolved models of volume increment of trees. The aim of this study is to combine these data and apply a root-development model to the aboveground part of trees. Three spruce trees (*Picea abies*) and two firs (*Abies alba*) which were part of a long-term forest monitoring survey were scanned using a terrestrial 3D-laser-scanner. Combining these data with tree-ring measurements, we were able to reconstruct stem volume at an annual resolution. Results provide robust annually resolved volume data along with ring-width measurements at any point within the modeled tree stem, which present great potential for complex growth analyses. Stem volume, estimated with a bole volume function, deviated between -1.65 and 1.9% from our model for four out of five trees. For the fifth tree deviations of 13% were observed. The agreement between the function and our model demonstrates the robustness of the presented approach.

Introduction

Forests provide crucial ecological and socio-economic functions and play a key role in the global carbon cycle (Dixon et al. 1994; Führer 2000; Gooddale et al. 2002; Dobbs et al. 2011; Miura et al. 2015). Information on tree biomass and volume is needed for sustainable forest management and to understand and quantify nutrient flows in ecosystems (Zianis et al. 2005). Precise data on tree volume, increment and growth development at the national level can allow for efficient forest management and controlling (Kleinn 2002) and in turn enables reliable quantification of CO_2 sequestration at a broader scale. Thus, models providing reliable biomass or volume estimates at a national scale are needed. So far techniques to assess forest biomass have mainly been based on allometric equations (Fehrmann and Kleinn 2006). These formulas rely on the indirect relationship between tree attributes such as diameter at breast height (dbh), tree height and volume (Zianis et al. 2005; Calders et al. 2015). Allometric equations are usually site specific, species specific or only representative for certain diameter classes, and thus not applicable at a broader scale (Muukkonen 2007; Liang

⌂ Springer

et al. 2014). Although the volume estimates based on dbh generally lead to larger errors compared to those also measuring tree height or an diameter at other heights (Kaufmann 2001; Dassot et al. 2011; Liang et al. 2014), in many forest inventories only the dbh is assessed, to reduce the workload (Köhl 2001; Liang et al. 2014).

Terrestrial laser scanning (TLS) is a new technique that has gained popularity since the beginning of the twenty-first century (Maas et al. 2008; Kankare et al. 2014). TLS can assess detailed information of several trees in a short period of time and is regularly applied in forestry (Dassot et al. 2011, 2012; Srinivasan et al. 2015; Seidel et al. 2011; Calders et al. 2015). Although point cloud processing might be time consuming (Brenner 2007), TLS is an effective tool to assess tree architecture and stand structure. It enables direct estimates of individual tree volume (Calders et al. 2015), allows for the extraction of typical terrestrial inventory parameters such as tree height and dbh (Dassot et al. 2011; Kankare et al. 2014) and for modelling the 3D-structure of trees. Using diameter approximation techniques of fitting b-splines or circles to the point clouds (Pfeifer and Winterhalder 2004; Bienert et al. 2006; Wang et al. 2017), it is possible to measure the diameter at different heights (Pfeifer and Winterhalder 2004; Kankare et al. 2014). The tree surface characteristics can also be approximated either manually or automated for individual trees, tree parts (roots/branches) or entire stands (Raumonen et al. 2013, 2015) by triangulating the point cloud to a closed surface (meshing/triangulation) (Aschoff et al. 2004; Wagner et al. 2011a), by fitting cylinders to the point clouds (Pfeifer and Winterhalder 2004; Othmani et al. 2011; Åkerblom et al. 2012; Raumonen et al. 2013; Hackenberg et al. 2014, 2015b) or by transferring the point clouds into voxel models (Lefsky and McHale 2008). Although scans seem to depict the stand in a realistic way, scanner data also deviate from reality. Some typical error sources such as registration errors, occlusion effects and the assessment of small artifacts due to the scanning accuracy itself occur (Pfeifer and Winterhalder 2004; Kankare et al. 2013; Raumonen et al. 2013; Liang et al. 2014; Calders et al. 2015). Usually, laser scanning data slightly overestimate diameters and volume (Henning and Radtke 2006). A registration error of 1 cm can potentially lead to a volumetric overestimation of 8.8% (Burt et al. 2013). The strong effect of small differences in dbh determination on volumetric data illustrates the need for an additional parameter to validate scanner data. Furthermore, most methods only represent a current state of trees and do not show volume development over time and hence, the annual volume increment of trees. Only one study we know of used volume data derived from crown shapes assessed by airborne laser scanning and combined them with ecosystem modeling approaches to estimate annual wood increment on the basis of forest net primary production, carbon stem allocation ratios, the volume biomass expansion factor, and the basic wood density (Bottai et al. 2013). However, the growth development of trees in 3D for comprehensive growth analyses is still lacking full understanding of carbon sequestration and allocation within trees. Currently, to assess volume changes from laser scans, stands need to be frequently scanned (Liang et al. 2012; Sheppard et al. 2017), which limits the time period over which volume development can be assessed.

In contrast, tree-ring data show the annual development of tree increment over time, but lack additional information about tree ring and volume evolution in a three dimensional manner. Some approaches to estimate tree volume based on tree-ring data exist. For instance, Babst et al. (2014) first reconstructed the historic diameters and then applied allometric equations to derive annual growth increment. However, their approach does not show the development of tree volume increment in 3 dimensions. Moreover, they still rely on species-specific allometric equations. Others developed growth and volume equations based on tree-ring analysis for teak (Perez 2008) or derived tree height curves from tree-ring data (Carmean 1972). None of them provides detailed 3D growth information. The combination of highly accurate tree-ring width data and point-cloud data from terrestrial laser scanning fills this research gap and allows for a robust 3D reconstruction of annually resolved volume and allocation patterns. While tree-ring data contain growth information with an accuracy of 1/100 mm and an annual resolution TLS data provide a 3D model representing the surface and structure of trees at a certain point in time.

Wagner et al. (2011a) proposed for the first time a model that combines both highly accurate tree-ring width data and 3D point-cloud data from terrestrial laser scanning. They applied their model to the belowground part of trees and demonstrated that it is a robust method for 3D-modeling of tree-root systems, but it was never applied to the aboveground part of trees. For roots, the model showed an overestimation of 3.5–6.6% compared to reality and was expected to be more accurate for simpler shapes such as tree stems (Wagner et al. 2011a). A spatio-temporal context is needed for tree stem modelling, which is species independent.

Therefore, the aims of this study are as follows:

1. To apply the coarse-root model developed by Wagner et al. (2011a) to the aboveground part of five trees and to reconstruct the annual volume increment in combination with tree ring-width data.
2. To compare the total stem volume derived by the model with volumetric equations used in the Swiss National Forest Inventory (NFI).

Materials and methods

Study site

Long-term sample-plot inventory has been carried out by the NFI in the forest of Bremgarten, Switzerland in the years 1971, 1986, 1996 and 2011 according to the method of Schmid-Haas and Werner (1969). Two stands were selected from this long-term sample-plot inventory one dominated by Spruce (*Picea abies* (L.) Karst.), and a second dominated by Fir (*Abies alba* Mill.) mixed with larch (*Larix decidua* Mill.). Five individual trees, three Spruce and two Fir trees, situated within the two sample plots were selected for the investigation. The samples were also assessed during the long-term sample-plot inventory.

Terrestrial laser scanning

The stands were scanned in autumn 2011 following the growing season. Scanning targets were distributed in the forest stands covering the inventory plots for later registration of the individual scans. Both plots (radius of 12.5 m) were scanned with a terrestrial laser scanner (Leica ScanStation C10). The scanner assesses the aboveground structure of trees with a laser footprint. The surface of trees is represented by individual points in a Cartesian coordinate system

(xyz) (Fig. 1). The Leica ScanStation C10 scans with a resolution of up to 50,000 points/s. The spot size is 4.5 mm Full width at the half-height-based and 7 mm Gaussian-based. The minimum spacing is < 1 mm (Leica Geosystems AG Heerbrugg, Switzerland). The scanning resolution for this study was 5 mm point distance per 10 m distance. On average the distance between scanner and the individual trees was 7.5 m. Thus, the average point distance for the single scans of this study was 3.5 mm. This resolution was used for all scans. The scanner was positioned on a tripod to assess 360° scenes. To minimize occlusion effects, multiple scans were taken to assess the full 3D tree structure and the laser scanner shifted 4–5 times on each plot. In this way, each tree was covered from at least four sides. The single scans were geo-referenced using the Cyclone software (Fig. 1; Leica Geosystems, version 7.3.3). Point clouds of individual trees were later manually extracted from their surroundings and transferred into the software Geomagic (Geomagic Studio, 2011, http://www.geomagic.com). After scanning, the trees were harvested and cut into segments to allow for the subsequent ring-width measurements.

To reconstruct the annual volume of trees three input data sets are needed from Geomagic: (1) the 3D structure of the tree stem; (2) the cross sections of the 3D stem representing the outer shape of the real cross sections at which the tree-ring data were measured; and (3) two points representing
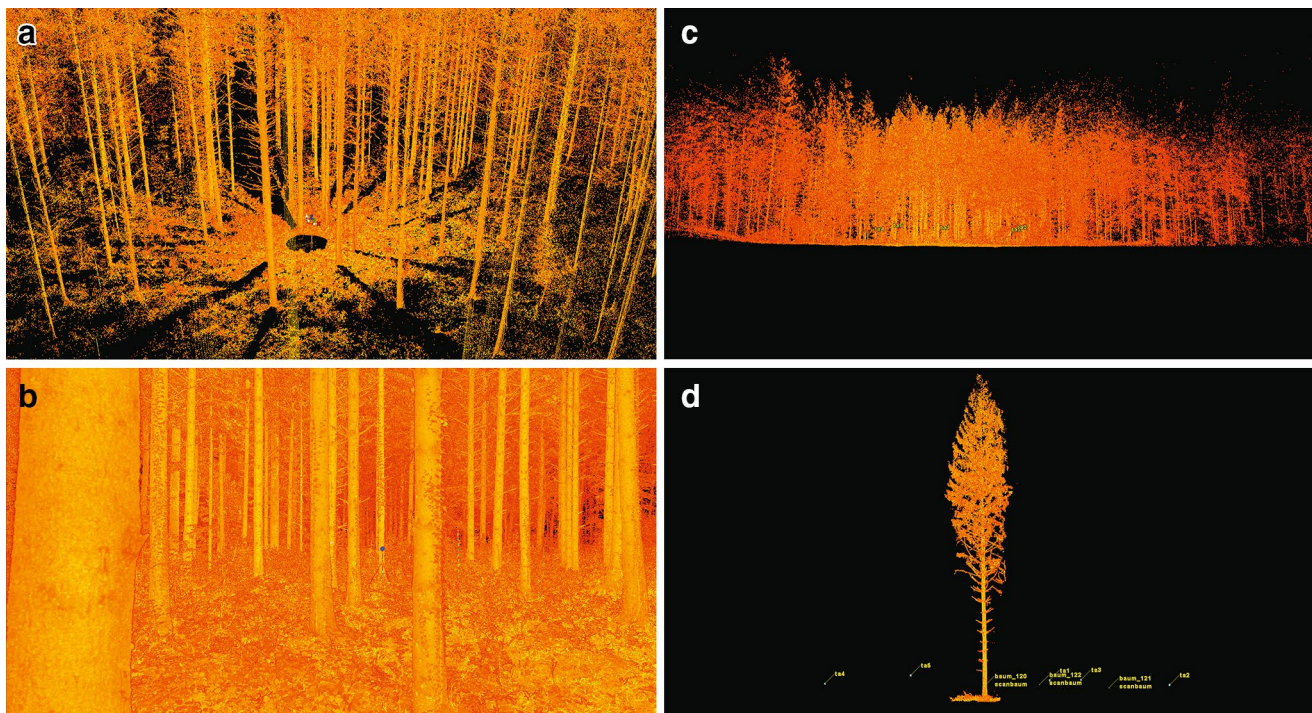

Fig. 1 The point cloud data assessed with a terrestrial laser scanner **a** point cloud of a single 360° scan (average no. of points: 13,500,000) **b** close up of a single scan with one of the reference targets in the center **c** multiple scans (4–5) referenced with the Cyclone software **d** individual tree manually separated from the stand data (average no of points: 3,900,000)
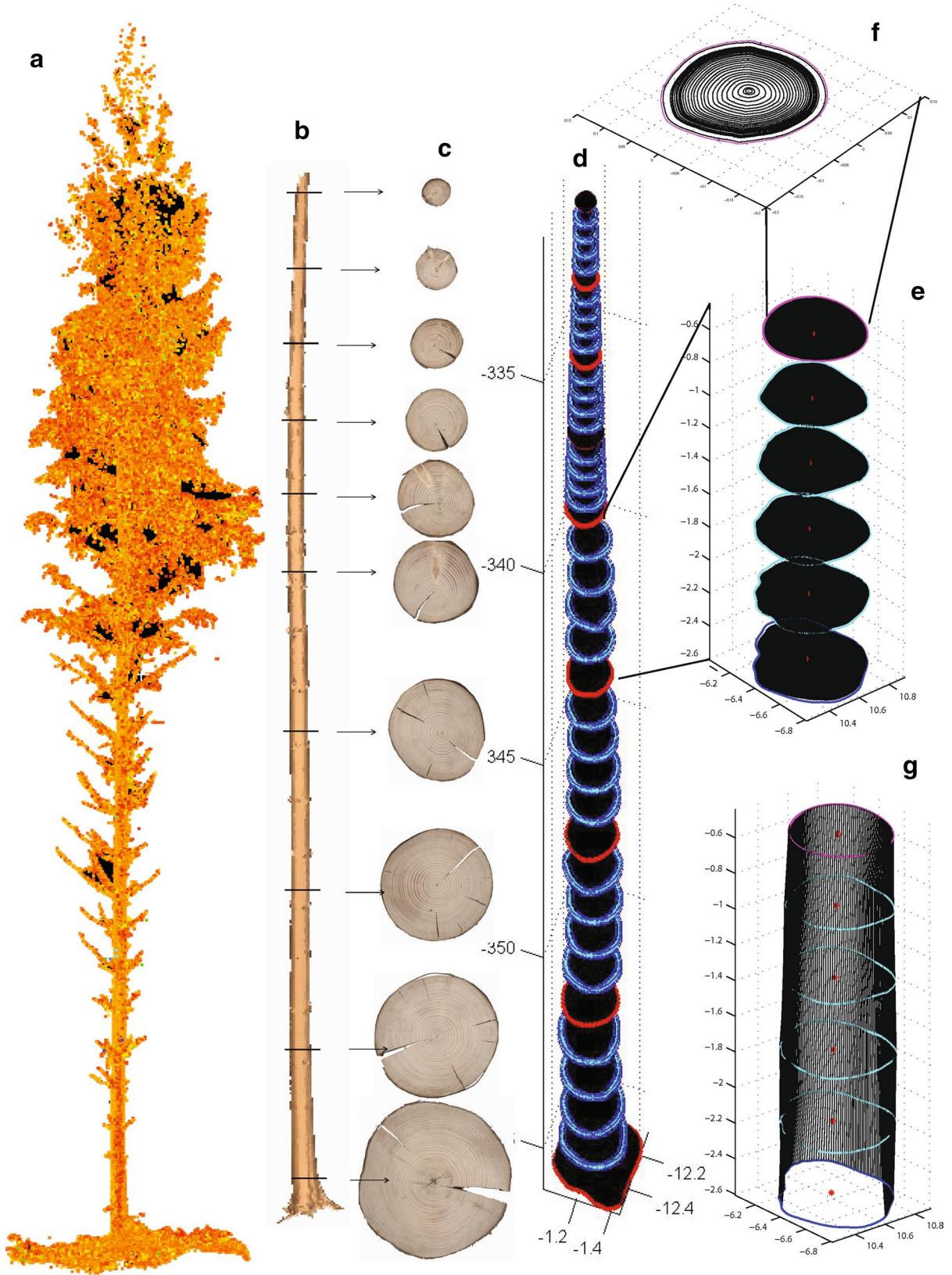
the starting points of the two first measured tree-ring radii per cross section on the stem surface (Wagner et al. 2011a, b; Santini and Wagner 2010). All these data were saved in ASCII format containing the Cartesian XYZ coordinates of these points.

Erroneous points were removed from the laser point clouds using cutting tools and additional filters provided by Geomagic. Branches were manually removed from the scan. Due to the dense canopy of conifers the laser could not assess the upper stem completely, and thus data points are missing from the upper part of the stem. To approximate the stem shape at the upper part of the stem, cylinders or cones were manually fitted to the point cloud. Afterwards, the distortion free point cloud was triangulated and transferred into a 3D mesh surface model (Remondino 2003). The results were manually checked and—if necessary—filters (mesh doctor) and curvature based filling were applied using Geomagic. As a second data set, the circumferences of the cross sections were extracted. Using the curve extraction function in Geomagic 2011 cross sections were cut out of the model exactly at the position where the respective stem cross sections were taken in reality. The resulting digital cross sections are line segments and were again transferred into a point file (.xyz). From these points representing the outer shape of the cross section two points were extracted representing the starting point of the measured tree-ring radii and also saved as .xyz files. The mesh was retransferred into an ordered point cloud as required by the 3D modeling tool of Wagner et al. (2011a).

Tree-ring data

Cross sections were cut in a perpendicular angle from the stem. From the base up to a height of 16 m a section was taken every 4 m, above this height towards the top every 2 m. The lowest and highest measured cross sections for each tree are given in Table 2. The disks were sanded, polished and then scanned with a distortion-free flatbed scanner. Ring-width measurements were realized on the resulting digital images along four radii per disk according to standard dendrochronology techniques (Cook and Kairiukstis 1990) using WinDENDRO software (Regent Instruments Canada

Inc. 2009). In general, radii were measured at a 90° angle to each other, but in cases of cracks or deformations the angle was adapted. Data were saved as .txt files containing the ring widths in mm with an accuracy of 1/100 mm (Regent Instruments Canada Inc. 2009).

3D stem reconstruction

The input data for the 3D root model programmed in MATLAB by Wagner et al. (2011a) are the WinDENDRO files (.txt) and the Geomagic data sets [the outer shape of the trees (.xyz) as described above, the circumference of the cross sections (.xyz) and the starting points of the radii (.xyz)].

A weighted interpolation algorithm is used to compute cross sections at any point within the model to obtain growth layers. In a first step the model integrates the measured tree-ring radii into the 3D point cloud of the stem using the two starting points of the first measured radii on the stem surface as reference points. Using trigonometry the four input radii are reconstructed on the cross sections of the 3D tree model (as generated in Geomagic). From the tree-ring measurements the overall lengths of the input radii are known. In combination with the starting points of the first two input radii, enough parameters are known to reconstruct the four radii into the model. Due to the known offset of the 3D surface model, which is slightly larger than the actual tree stems, an algorithm centers the complex of the four radii within the model. Otherwise a one-sided bias would occur. In this way, the offset can be excluded later without biasing the volume reconstructions. Thus, the offset is not affecting the accuracy of the ring-width data. Thereafter, the 2D tree-ring profiles are interpolated in RootLAB on the input cross sections between the measured radii. A weighted interpolation algorithm is used. Radii are calculated with a resolution of 1° on a polar grid centered at the pith, but the angle can individually be adjusted. Thus, 356 new radii are interpolated between the four input radii. For each radius the point of intersection with the circumference of the cross section is calculated, given the distance between the pith and the circumference. This distance later accounts for the individual shape of the tree stem as this distance varies along the circumference. To reconstruct the ring widths for the new radii, ratios for all the input radii are calculated giving a measure for the distances of a specific ring border to the bark with respect to the total length of the radius. The closer a new calculated radius is to one of the input radii the more weight is put on the corresponding ring width and thus, the ratio of the closer input radius This weighted approach allows for a highly precise approximation of ring profiles (details in Wagner et al. 2011b). At this point the tree-ring profiles of the input cross sections are fully reconstructed (Fig. 2d—the red cross sections). Thereafter, the annual growth layers are interpolated in 3D. For this calculation, a correspondence between two adjacent input cross sections is required. Several anchor

points are calculated between two adjacent cross sections and also with the 3D stem model. To this end, a plane is calculated passing through the pith of two adjacent input cross sections and the intersection point of the first input radius with the circumference of the first cross section. The intersection point of the plane with the circumference of the second cross section is now referred to as radius one from cross section two. In the following, the plane rotates with a resolution of 1°, recomputing the tree rings on cross section two as described before, resulting in the same polar grid. In this way, radius one of cross section one corresponds directly to radius one of cross section two and so on. This is done for all adjacent cross sections. In a next step new cross sections are required between the input cross sections. By default four cross sections are evenly distributed between each set of input cross sections, but the number can be enhanced depending on the complexity and curvature of the stem. As the input cross sections are not truly parallel, the orientation of the new cross sections is set to be a weighted average between the orientations of the two adjacent cross sections. To calculate the ring profiles on the new cross sections the growth center (pith of each cross section) is calculated as an anchor point for later tree-ring reconstructions. Again it is approximated by calculating the radii lengths as a weighted average considering the corresponding radii lengths at the input cross sections with respect to the relative distance of the new cross section to the two input cross sections. The growth center is finally approximated as the average of all these distances and the new pith is used as the center of the polar grid for the new reconstructions. Again, the closer one of the new calculated cross sections is to the input cross sections, the greater the tree-ring width of the input cross sections is weighted for the corresponding growth year [see Wagner et al. (2011a, b) and Santini and Wagner (2010) for details]. At this point the new cross sections are fully reconstructed (Fig. 2d, e) and growth layers can be computed between the cross sections (Fig. 2g). The volume of the individual growth layers is now calculated for single sectors and then summed for the entire tree. These sectors are geometric bodies. In general a prism is calculated, with a trapezoid base area only for the sectors of the first growth ring. Thus, these sectors are limited by two adjacent cross sections, two neighboring radii with an angle of 1° at the pith and two successive growth-ring borders. Later all sectors for a corresponding growth year are summed up. Due to the small angle of 1° between radii the volume error seems to be negligible and a convenient approximation. Thus, the output data of the model are the annual tree-ring data at any point within the modelled tree stem and the annually-resolved

volume data. Figure 2 exemplifies the single steps of the workflow including the modeling procedure for one tree stem. The relevant parameters for the final modeling of the two Fir trees and the three Spruce trees such as dbh and height are listed in Table 2.

Volume equations

Over bark bole volume function

The over bark volume function of the NFI, which is based on the tree structure parameters tree height, and two diameters at 1.3 and 7 m height, was used for the validation of our model. Species-specific allometric equations for bole volume including bark (Eqs. 1, 2) were derived together with seven other equations following assessment of more than 38,000 trees in the framework of the NFI. Additionally, 500 trees of different species with extreme parameter ratios were measured (Kaufmann 2001). As precise data are required for large-scale inventories there is a need to measure all the parameters for at least some trees (Kaufmann 2001).

$$\text{Spruce:} \quad Y = b_0 + b_1 \times d_7^2 H + b_2 \times d_{1.3}^2 + b_3 \times d_7^3 + b_4 \times H \quad (1)$$

$$\text{Fir} : \quad Y = b_0 + b_1 \times d_7^2 H + b_2 \times d_{1.3} + b_3 \times d_{1.3}^2 \\ + b_4 \times d_{1.3}^3 \times H + b_5 \times H^4 \quad (2)$$

where: Y: bole volume including bark, $D_{1.3}$: diameter at breast height in meters, D_7: diameter at 7 m height in meters, H: tree height in meters.

The coefficients of the bole volume function are listed in Table 1.

Results

The application of the root-growth model originally developed for coarse roots, to the aboveground parts of trees was possible without modifications for stems. Combining the ring-width measurements and the TLS data allowed for a detailed analysis of the annual ring and volume development of all five trees (Fig. 3).

Although the overall dimensions of the sample trees were comparable (despite dbh of F1; see Table 2), the two fir trees (F1, F2) were more than 100 years old, while the spruce trees (Sp1–Sp3) were less than 50 years of age. When combining the tree-ring data with the 3D model,

Table 1 Coefficients of the bole volume function (Kaufmann 2001)

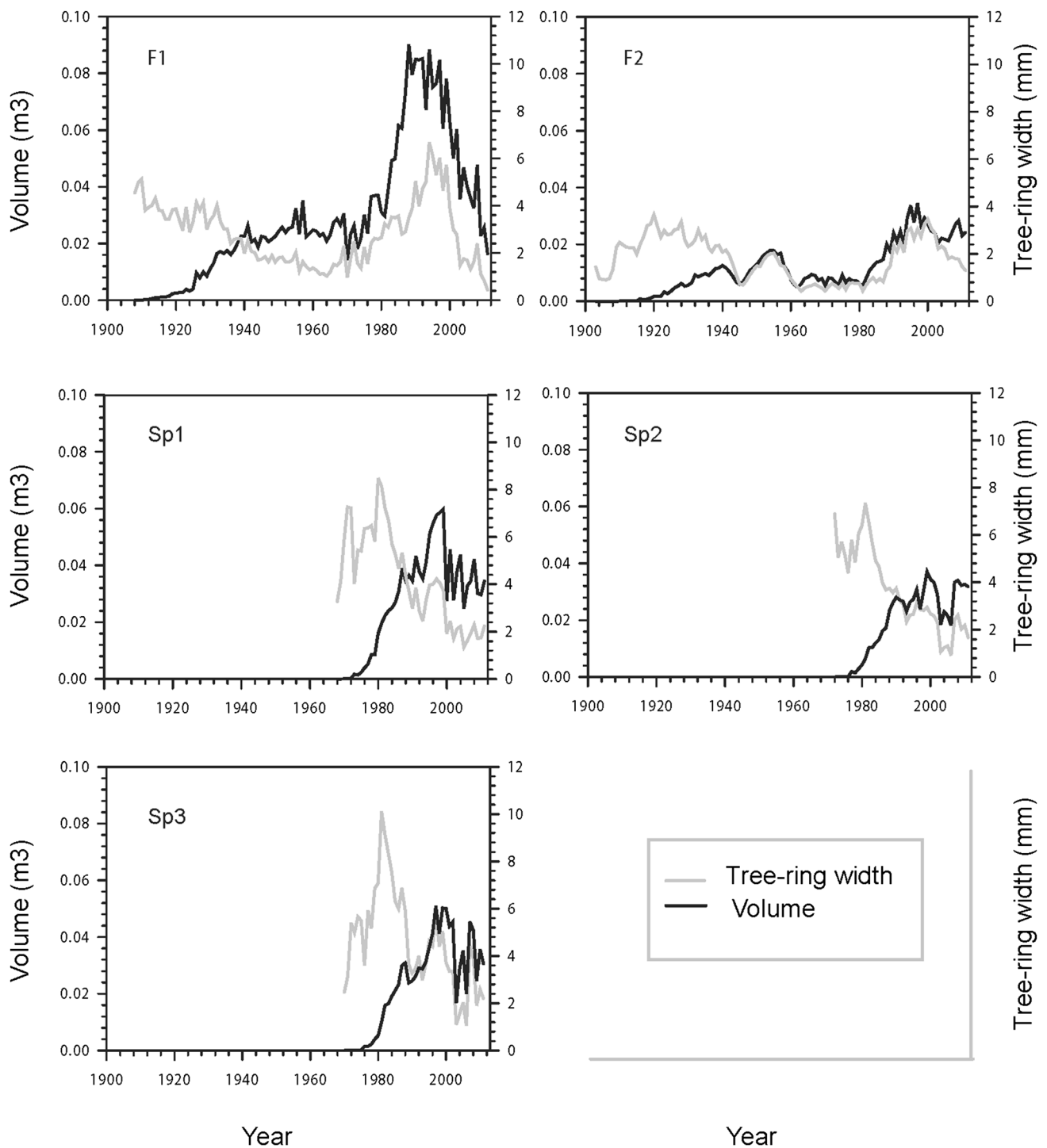| Species	b0	b1	b2	b3	b4	b5
Spruce	0.029504	0.46756	2.43885	− 5.74664	− 0.001826	
Fir	0.039594	0.35832	− 0.39142	3.75195	− 0.013314	1.62E−07

Fig. 3 Annual tree-ring width plotted against annual volume accumulation of two Firs and three spruces

there were also differences in volume accumulation in spruce and fir. Focusing on the total stem volume, there is a clear difference between the species (Fig. 4). Volume accumulation in spruce reached around 1 m³ within 40 years, while the fir trees reached this volume after 60 years (F1) and 100 years (F2), respectively (Fig. 4).

For the last decade, there was a clear decrease in ring width in fir, which was also visible to a lesser extent in the spruce trees. Despite the declining ring width the cumulated volume increased for all trees. When plotting the annual volume and ring-width increment (Fig. 3), both show a decline, although it is less pronounced for

Springer

Table 2 Tree characteristics

TreeID	Species	Total tree		CS (lowest)		CS (highest)	
		*d*1.3 (cm)	Height (m)	Ø (cm)	Height (m)	Ø (cm)	Height (m)
F1	*Abies alba*	63	34.44	60.43	0.77	15.03	32.1
F2	*Abies alba*	37	32.19	36.12	0.25	7.85	27.05
Sp1	*Picea abies*	33	30.38	38.62	0.9	7.15	27.73
Sp2*	*Picea abies*	28	27.79	31.51	0.67	(a) 7.78	23.67
						(b) 8.22	
Sp3	*Picea abies*	37	29.39	47.88	0.1	8.92	24.88

d1.3 diameter at 1.30 height, CS cross section, ID identity

*Forked stem from ~ 15 m height towards top

volume increment. The annual volume increment of F2 even increases in the last decade (Fig. 3). Forest inventory data indicate that the growing conditions were different between the firs and the spruces. The firs grew by natural regeneration on a site initially planted with larches following clear cut. Due to competition with the older larches their juvenile growth was slow but following harvest of the dominant larches in 1960, F1 experienced a growth release becoming dominant growing without competition. The growth decline starting in the 1990s cannot be explained by competition. The second fir (F2) growing at the same site was further dominated by larches and firs and never became dominant. The differences are very well expressed in the growth patterns.

The spruce site on the other hand was cleared due a storm in 1967 and then afforested by spruce, most likely with a high stand density (distances 1 × 1 m). The stand was regularly thinned. The inventory data show that the samples trees always belonged to the dominant canopy class, which also explains why they were initially able to grow comparatively quickly. In any case, Sp1–3 were always in competition with surrounding trees to a lesser or greater degree. Sp1 and Sp3 accumulated volume faster than Sp2. Clearly, Sp3 experienced less competition than Sp1 and Sp2. However, the competition experienced by Sp1 and Sp2 seem to be comparable. Further conclusions on whether the differences are caused by the forked structure of Sp2 or their different competitive abilities cannot be drawn from the data.

Figure 5 shows the height development of all trees. While all Spruces reached a height of about 20 m after 20 growth years the Firs only reached this height after between 40 and 45 growth years (Fig. 5). The comparison with the Swiss NFI data showed that the bole volume function of the NFI agreed with our model for 4 out of 5 trees with model deviations between − 1.65 and 1.9%. For the fifth tree (F2, Table 3) a volume difference of − 13% was observed. As an additional validation step for this particular tree (F2) we computed the truncated cone volume for all its stem segments and summed them. The sum of the truncated cone volume deviated by only 3.59% from our model. The laser

scans in our study overestimated tree volume by 11.27, 12.11, 12.74, 13.17, 13.90% when considered alone without the tree-ring information.

Discussion

The 3D model was applied to the aboveground part of trees and allowed for successful reconstructed of the annual and total stem volume of five trees. We reconstructed reliable data describing annual volume development of trees in combination with ring-width data for tree stems. This model allows for complex growth development analyses, which represents a significant progress over 3D models that can only capture stem volume for a specific moment in time (Dassot et al. 2012; Burt et al. 2013; Kankare et al. 2014; Calders et al. 2015). Moreover, until now TLS stem volume was reconstructed with errors ranging from − 7.85% (Hackenberg et al. 2015a, b) to 15.3% (Kankare et al. 2013) for solid stem wood, and 22.1% root mean-square error (RMSE) for saw wood, 110% RMSE for pulp wood (Kankare et al. 2014), and 8% for total tree above ground volume (Hackenberg et al. 2015b). Most of these models overestimate the actual stem volume. For volumes directly derived from the dbh measured from TLS data, which is a method commonly used in practice, this overestimation seems to be caused by the fact that small variations of the dbh result in large variations in the volume determination. According to Burt et al. (2013) registration errors of 1 cm resulted in an 8.8% volumetric overestimation of the stem. The laser scans in our study also overestimated tree volume by 11–14% when considered alone without the tree-ring information.

We expected that the combination of laser scans and high precision tree-ring data would be able to compensate for the known overestimation of the terrestrial laser scans and minimize the estimation error of laser scans. The model was previously calibrated and validated for coarse roots. Although these roots did not have simple, more or less round shapes as most tree stems do, the overestimation of 3.5–6.6% determined for these roots (Wagner et al.
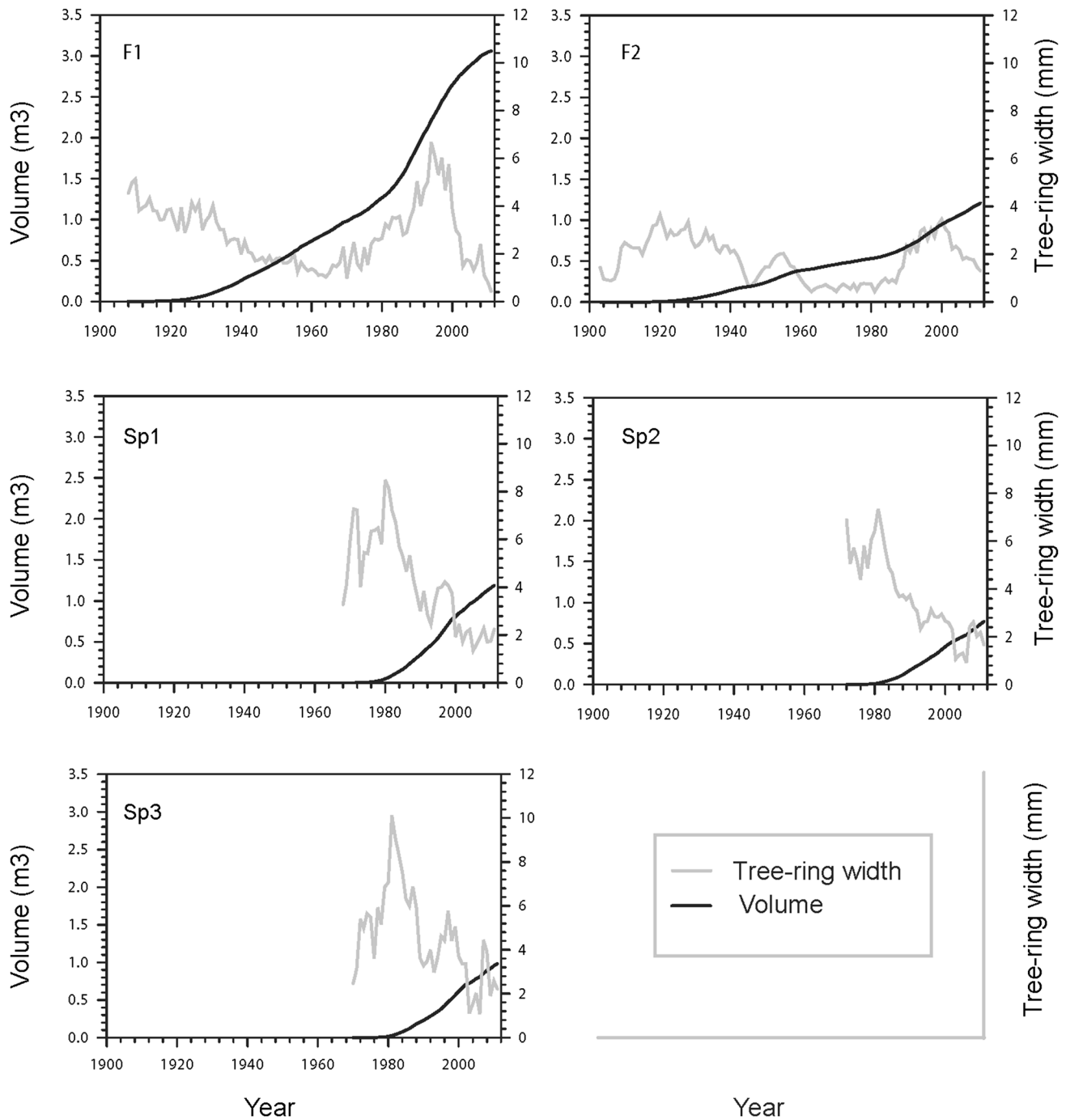
Fig. 4 Annual tree-ring width plotted against the accumulated volume development of two Firs and three spruces

2011a) are below most of the estimation errors from previous studies time (Dassot et al. 2012; Burt et al. 2013; Kankare et al. 2013, 2014; Calders et al. 2015; Hackenberg et al. 2015b). The model might, therefore, be expected to be even more accurate for simpler shapes such as tree stems (Wagner et al. 2011b). The bole volume functions of the NFI may provide additional information about the accuracy of our model as an additional diameter at 7 m

height is measured, which is in general more precise than those functions relying on only DBH measures (Kaufmann 2001; Dassot et al. 2011; Liang et al. 2014). As the bole volume function widely agreed with our model with deviations between 0.4 and 1.91% for four trees it strengthens the robustness of our model. Only for tree F2 bigger deviations of − 13.4% occurred (see Table 3). However, as the sum of the truncated cone volume for the same tree
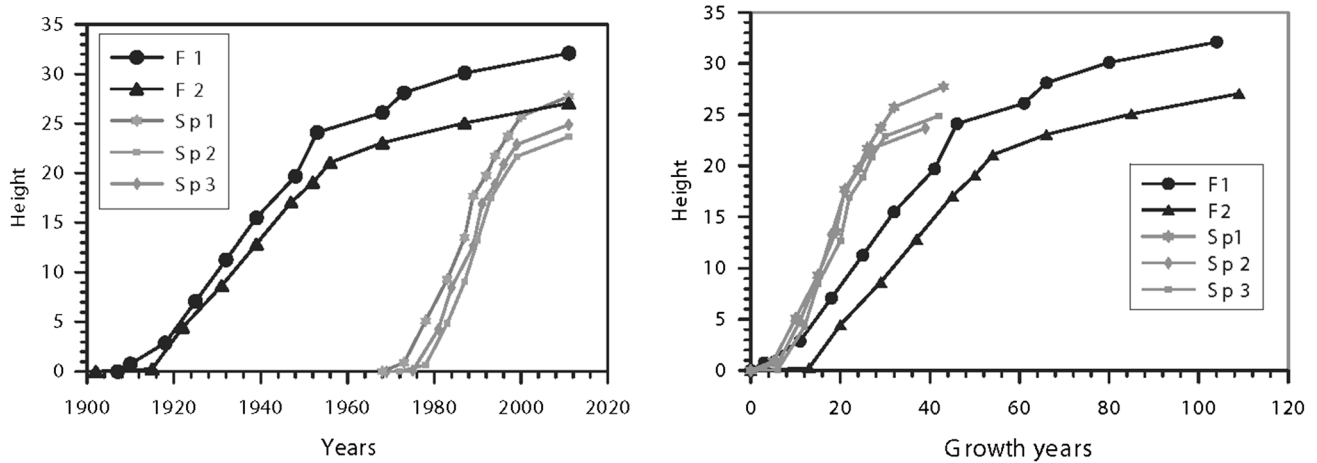
Fig. 5 Annual height development of the five modeled trees per year and growth year

Table 3 Bole volumes of RootLAB and the Bole volume functions with volume deviations between the 3D model and the functions

Tree ID	Volume in (m³)			Deviation RootLAB with Bole volume function in (%)
	Overbark Bole volume function[a]	3D model	3D model + stump	
F1	3.87	3.26	3.92	1.24
F2	1.54	1.32	1.33	− 13.40
Sp1	1.35	1.20	1.36	1.91
Sp2[b]	0.83	0.77	0.81	− 1.65
Sp3	1.19	1.05	1.18	− 0.40

[a]Input parameters (h, d1.3, d7)

[b]Forked stem

deviated by only 3.59% from our model it also strengthens our model.

The advantage of our model is that it relies not only on the laser scans or inventory parameters such as dbh or height, but also combines them with high precision tree-ring data. Thus, overestimation of volume due to scanning or registration errors does not bias the results of our model. Overestimated volume is directly excluded from volume calculations and as such does not affect the annually resolved volume data (Wagner et al. 2011a). In addition, our model takes the unique shapes of trees into account as trees are often not centric. A cylindrical fit may not always be a proper approximation, particularly for the lower part of a stem which contain a higher proportion of woody biomass (Calders et al. 2015). Using geometrical objects, the shape of a tree can only be approximated and abrupt diameter changes or anomalies cannot be properly assessed (Eysn et al. 2013). For the lower 6 meters of stems, volume differences between meshing and cylinder fitting ranged between − 3.6 and 5.5% (Dassot et al. 2012). Due to occlusion effects we also fitted cylinders to the upper part of the stems, but preserved the more variable part of the stem, which partly explains the robustness of our model. To a certain extent our model also accounts for stem sweep as the orientation of the interpolated cross sections are always calculated as a weighted average between the orientations of the two adjacent cross sections. In addition, the number of calculated cross sections between the interpolated cross sections can be enhanced in highly variable stem sections (Wagner et al. 2011a). However, if the stem shape is highly variable between two cross sections the model may deviate significantly from actual stem volume.

All volume models and carbon assessment approaches are subject to trade off between accuracy and workload. However, parameter reduction is only a feasible instrument if it is not at the expense of accuracy. Therefore, an accurate reconstruction of growth development is needed to verify allometric equations. Destructive sampling is generally required to calibrate allometric biomass models (Calders et al. 2015). Although laser scanning assesses in a short period of time point clouds of entire stands the workload of generating an error free surface model from laser scans is still time consuming. We have observed that the engineering software for point clouds improved significantly during the last years and thus, workload will be successively reduced for our model.

Several researchers have already automatically extracted the circumference of tree sections for dbh computations or total tree stems (Raumonen et al. 2013, 2015; Srinivasan et al. 2015) which may also reduce the workload of our model in future. In addition, open-source software solutions for point-cloud processing have entered the market, such as Meshlab (Cignoni et al. 2008) and CloudCompare (Girardeau-Montaut 2016), which are reducing the expenses for laser scanning and open the technique to a broader audience. Some open-source software have been developed specifically for tree reconstructions and forestry applications (Computree, Simple tree, 3dforest; Othmani et al. 2011; Hackenberg et al. 2015b; Trochta et al. 2017), but so far none combines these data with annual growth information. A disadvantage of our model remains the destructiveness of the approach. However, we believe that we first need reliable data to reconstruct the annual volume of a tree in a robust way to later be able to derive and validate good approximation methods. A step towards limiting the workload and destructiveness of our method would be reducing the number of tree-ring data required using tree cores only. One of the major challenges in this approach would be including height development in a realistic way.

Conclusions

We show that an existing 3D root volume model is applicable to the aboveground part of trees. The model reconstructs the volumetric stem development of trees over time at an annual resolution. As our model combines laser scanning data with highly accurate tree-ring data and it compensates for overestimations of laser scans. This allows for a highly precise reconstruction of annually resolved volume data of the stem and also for roots and branches. An additional advantage of our model is that it is species and site independent. The application to all woody parts allows for complex allocation patterns within a tree. A disadvantage is still the destructiveness and the time demanding reconstruction of the point clouds. However, work towards automated reconstruction of stems from laser point clouds is already in progress.

References

Åkerblom M, Raumonen P, Kaartinen H (2012) Comprehensive quantitative tree models from TLS data. In: Proceedings of the geoscience and remote sensing symposium (IGARRS) 2012 IEEE international, pp 6507–6510. doi:10.1109/IGARSS.2012.6352751

Aschoff T, Thies M, Spiecker H (2004) Describing forest stands using terrestrial laser-scanning. Int Arch Photogramm Remote Sens Spat Inf Sci 35:237–241

Babst F, Bouriaud O, Papale D, Gielen B, Janssens IA, Nikinmaa E, Ibrom A, Wu J, Bernhofer C, Köstner B, Grünwald T, Seufert G, Ciais P, Frank D (2014) Above-ground woody carbon sequestration measured from tree rings is coherent with net ecosystem productivity at five eddy-covariance sites. New Phytol 201:1289–1303. doi:10.1111/nph.12589

Bienert A, Scheller S, Keane E, Mulloly G, Mohan F (2006) Application of terrestrial laser scanners for the determination of forest inventory parameters. In: Maas H-G, Schneider D (eds) Proceedings of ISPRS commission V symposium 'Image engineering and vision metrology' 36. Part 5. ISPRS, Dresden

Bottai L, Arcidiaco L, Chiesi M, Maselli F (2013) Application of a single-tree identification algorithm to LiDAR data for the simulation of stem volume current annual increment. J Appl Remote Sens 7:073699–073699. doi:10.1117/1.JRS.7.073699

Brenner C (2007) Interpretation terrestrischer Scandaten. In: Beiträge zum 74.DVW-Seminar Terrestrisches Laser-Scanning, Band 53. Fulda, Germany, pp 170–179

Burt A, Disney MI, Raumonen P, Armston J, Calders K, Lewis P (2013) Rapid characterization of forest structure from TLA and 3D modelling. In: Proceedings of the geoscience and remote sensing symposium (IGARRS) 2013 IEEE international, pp 3387–3390. doi:10.1109/IGARSS.2013.6723555

Calders K, Newnham G, Burt A, Murphy S, Raumonen P, Herold M, Culvenor D, Avitabile V, Disney M, Armston J, Kaasalainen M (2015) Nondestructive estimates of above-ground biomass using terrestrial laser scanning. Meth Ecol Evol 6:198–208. doi:10.1111/2041-210X.12301

Carmean WH (1972) Site index curves for upland oaks in the central states. For Sci 18:109–120

Cignoni P, Callieri M, Corsini M, Dellepiane M, Ganovelli F, Ranzuglia G (2008) MeshLab: an open-source mesh processing tool sixth Eurographics Italian chapter conference, pp 129–136. doi:10.2312/LocalChapterEvents/ItalChap/ItalianChapConf2008/129-136

Cook ER, Kairiukstis A (1990) Methods of dendrochronology—applications in the environmental science. Kluwer, Dordrecht

Dassot M, Constant T, Fournier M (2011) The use of terrestrial LiDAR technology in forest science: application fields, benefits and challenges. Ann For Sci 68:959–974. doi:10.1007/s13595-011-0102-2

Dassot M, Colin A, Santenoise P, Fournier M, Constant T (2012) Terrestrial laser scanning for measuring the solid wood volume, including branches, of adult standing trees in the forest environment. Comput Electron Agr 89:86–93. doi:10.1016/j.compag.2012.08.005

Dixon RK, Brown S, Houghton RA, Solomon AM, Trexler MC, Wisniewski J (1994) Carbon pools and flux of global forests ecosystems. Science 263:185–190. doi:10.1126/science.263.5144.185

Dobbs C, Escobedo FJ, Zipperer WC (2011) A framework for developing urban forest ecosystem services and goods indicators. Landsc Urban Plan 99:196–206. doi:10.1016/j.landurbplan.2010.11.004

Eysn L, Pfeifer N, Ressl C, Hollaus M, Grafl A, Morsdorf F (2013) A practical approach for extracting tree models in forest environments based on equirectangular projections of terrestrial laser scans. Remote Sens 5:5424–5448. doi:10.3390/rs5115424

Fehrmann L, Kleinn C (2006) General considerations about the use of allometric equations for biomass estimation on the example of Norway spruce in central Europe. For Ecol Manag 236:412–421. doi:10.1016/j.foreco.2006.09.026

Führer E (2000) Forest functions, ecosystem stability and management. For Ecol Manag 132:29–38. doi:10.1016/S0378-1127(00)00377-7

Girardeau-Montaut D (2016) Cloud Compare: 3D point cloud and mesh processing software, open source project. http://www.danielgm.net/cc/. Accessed 7 July 2017

Gooddale CL, Apps MJ, Birdsey RA, Field CB, Heath LS, Houghton RA, Jenkins JC, Kohlmaier GH, Kurz W, Liu S, Nabuurs GJ, Nilsson S, Shvidenko AZ (2002) Forest Carbon Sinks in the northern Hemisphere. Ecol Appl 12:891–899. doi:10.1890/1051-0761(2002)012[0891:FCSITN]2.0.CO;2

Hackenberg J, Morhart C, Sheppard J, Spiecker H, Disney M (2014) Highly accurate tree models derived from terrestrial laser scan data: a method description. Forests 5:1069–1105. doi:10.3390/f5051069

Hackenberg J, Wassenberg M, Spiecker H, Sun D (2015a) Non destructive method for biomass prediction combining TLS derived tree volume and wood density. Forests 6:1274–1300. doi:10.3390/f6041274v

Hackenberg J, Spiecker H, Calders K, Disney M, Raumonen P (2015b) SimpleTree—an efficient open source tool to build tree models from TLS clouds. Forests 6:4245–4294. doi:10.3390/f6114245

Henning JG, Radtke PJ (2006) Detailed stem measurements of standing trees from ground-based scanning lidar. For Sci 52:67–80 (ISSN 0015-749X)

Kankare V, Holopainen M, Vastaranta M, Puttonen E, Yu X, Hyyppä J, Vaaja M, Hyyppä H, Alho P (2013) Individual tree biomass estimation using terrestrial laser scanning. ISPRS J Photogramm Remote Sens 75:64–75. doi:10.1016/j.isprsjprs.2012.10.003

Kankare V, Vauhkonen J, Tanhuanpää T, Holopainen M, Vastaranta M, Joensuu M, Krooks A, Hyyppä J, Hyyppä H, Alho P, Viitala R (2014) Accuracy in estimation of timber assortments and stem distribution—a comparison of airborne and terrestrial laser scanning techniques. ISPRS J Photogramm Remote Sens 97:89–97. doi:10.1016/j.isprsjprs.2014.08.008

Kaufmann E (2001) Estimation of standing timber, growth and cut. In: Brassel P, Lischke H (eds) Swiss National Forest Inventory: methods and models of the second assessment. Swiss Federal Research Institute WSL, Birmensdorf, pp 162–192

Kleinn C (2002) New technologies and methodologies for national forest inventories. Unasylva 53:10–15

Köhl M (2001) Inventory Concept NFI2. In: Brassel P, Lischke H((eds) Swiss National Forest Inventory: methods and models of the second assessment. Swiss Federal Research Institute WSL, Birmensdorf, pp 19–44

Lefsky M, McHale M (2008) Volume estimates of trees with complex architecture from terrestrial laser scanning. J Appl Remote Sens 2(1):19. doi:10.1117/1.2939008

Liang X, Hyyppä J, Kaartinen H, Holopainen M, Melkas T (2012) Detecting changes in forest structure over time with bi-temporal terrestrial laser scanning data. Int J Geo-Inf 1:242–255. doi:10.3390/ijgi1030242

Liang X, Kankare V, Yu X, Hyyppä J, Holopainene M (2014) Automated stem curve measurement using terrestrial laser scanning

geoscience and remote sensing. IEEE Trans Geosci Remote Sens 52:1739–1748. doi:10.1109/TGRS.2013.2253783

Maas H-G, Bienert A, Scheller S, Keane E (2008) Automatic forest inventory parameter determination from terrestrial laser scanner data. Int J Remote Sens 29:1579–1593. doi:10.1080/01431160701736406

Miura S, Amacher M, Hofer T, San-Miguel-Ayanz J, Thackway R (2015) Protective functions and ecosystem services of global forests in the past quarter-century. For Ecol Manag 352:35–46. doi:10.1016/j.foreco.2015.03.039

Muukkonen P (2007) Generalized allometric volume and biomass equations for some tree species in Europe. Eur J For Res 126:157–166. doi:10.1007/s10342-007-0168-4

Othmani A, Piboule A, Krebs M, Stolz C, Lew Yan Voon LFC (2011) Towards automated and operational forest inventories with T-Lidar. In: 11th international conference on LiDAR applications for assessing forest ecosystems (SilviLaser 2011), Oct 2011. Hobart

Perez D (2008) Growth and volume equations developed from stem analysis for tectona grandis in Costa Rica. J Trop For Sci 20:66–75 (ISSN 0128-1283)

Pfeifer N, Winterhalder D (2004) Modelling of tree cross sections from terrestrial laser-scanning data with free-form curves. Int Arch Photogramm Remote Sens Spat Inf Sci 36:76–81

Raumonen P, Kaasalainen M, Åkerblom M, Kaasalainen S, Kaartinen H, Vastaranta M, Holopainen M, Disney M, Lewis P (2013) Fast automatic precision tree models from terrestrial laser scanner data. Remote Sens 5:491–520. doi:10.3390/rs5020491

Raumonen P, Casella E, Calders K, Murphy S, Åkerblom M, Kaasalainen M (2015) Massive-scale tree modelling from TLS data. ISPRS Ann Photogramm Remote Sens Spat Inf Sci 43:189–196. doi:10.5194/isprsannals-II-3-W4-189-2015

Remondino F (2003) From point cloud to surface: the modelling and visualization problem. Int Arch Photogramm Remote Sens Spat Inf Sci 34:5/W10

Santini S, Wagner B (2010) RootLAB: a matlab framework for the modeling of tree roots. Technical report no. 696. Department of Computer Science, ETH Zurich, Zurich, Oct 2010

Schmid-Haas P, Werner J (1969) Kontroll-Stichproben: Aufnahmeinstruktion. Bericht Eidgenössischer. Forsch Wald Schnee Landsch 27:22

Seidel D, Fleck S, Leuschner C, Hammett T (2011) Review of ground-based methods to measure the distribution of biomass in forest canopies. Ann For Sci 68:225–244. doi:10.1007/s13595-011-0040-z

Sheppard J, Morhart C, Hackenberg J, Spiecker H (2017) Terrestrial laser scanning as a tool for assessing tree growth. iForest 1:172–179. doi:10.3832/ifor2138-009

Srinivasan S, Sorin C, Popescu M, Eriksson R, Sheridan D, Ku NW (2015) Terrestrial laser scanning as an effective tool to retrieve tree level height, crown width, and stem diameter. Remote Sens 7:1877–1896

Trochta J, Krůček M, Vrška T, Král K (2017) 3D forest: an application for descriptions of three-dimensional forest structures using terrestrial LiDAR. PLoS One 12:e0176871. doi:10.1371/journal.pone.0176871

Wagner B, Santini S, Ingensand H, Gärtner H (2011a) A tool to model 3D coarse-root development with annual resolution. Plant Soil 346:79–96. doi:10.1007/s11104-011-0797-8

Wagner B, Gärtner H, Santini S, Ingensand H (2011b) Cross-sectional interpolation of annual rings within a 3D root model. Dendrochronologia 29:201–210. doi:10.1016/j.dendro.2010.12.003

Wang D, Kankare V, Puttonen E, Hollaus M, Pfeifer N (2017) Reconstructing stem cross section shapes from terrestrial laser scanning. IEEE Geosci Remote Sens Lett 2:272–276. doi:10.1109/LGRS.2016.2638738

Zianis D, Muukkonen P, Mäkipää R, Menuccini M (2005) Biomass and stem volume equations for tree species in Europe. Silva Fenn Monogr 4:63 (ISBN 951-40-1984-9)